Image deblur in gradient domain

Xiaogang Chen
Jie Yang
Shanghai Jiao Tong University
Institute of Image Processing and Pattern Recognition
China
Email: jhredblack@yahoo.com.cn

Qiang Wu
University of Technology
Centre for Innovation in IT Services and Applications
Sydney, Australia

Abstract. This paper proposes a new method for natural-image deblur based on a single blurred image. The natural image prior, a sparse gradient distribution, is enforced using a gradient histogram remapping method in the proposed deblur algorithm. The proposed objective function for blind deconvolution is solved by an alternating minimization method. The point spread function and the unblurred image are updated alternately. The proposed method is able to produce high-quality deblurred results with low computational costs. Both synthetic and real blurred images are tested in the experiments. Encouraging experimental results show that the newly proposed method could effectively restore images blurred by complex motion. [DOI: 10.1117/1.3505868]

Subject terms: motion deblurring; blind image deconvolution; image deconvolution; image enhancement.

Paper 100325RR received Apr. 14, 2010; revised manuscript received Jul. 28, 2010; accepted for publication Sep. 6, 2010; published online Nov. 10, 2010.

1 Introduction

Restoration of blurred images is an important task in image processing and computer vision problems. This paper focuses on spatially invariant image deblur and proposes a new method to estimate the *kernel* [point spread function (PSF)] and the *latent image* (original sharp image) from a single out-of-focus or motion-blurred image.

In the case of spatial invariance, the blurring process can be modeled by an image convolution operation.[1] When the PSF is given, the image can be restored by nonblind deconvolution methods, such as the inverse filter, Wiener filter,[1] Lucy-Richardson deconvolution (LR),[2,3] and maximum-likelihood estimation.[4] Most of these algorithms are reviewed and compared by Schuon and Diepold.[5] Since the precomputed PSF is inaccurate and the blurred image is also noisy in most real cases, nonblind deconvolution methods that are regularized by image priors have been popular in recent years.[6–9]

When the PSF is unknown, the image deblurring is commonly called *blind deconvolution*. The estimation is heavily underconstrained and sensitive to noise.[10] Therefore, more knowledge is required to improve the estimation conditions. Specifically, when the image is blurred by uniform linear motion, the PSF is determined by the motion direction and motion extent, which can be estimated from the power spectrum image[11] or by directional smoothness calculation and autocorrelation in the spatial domain.[12] For other motion-blurred or out-of-focus images, existing methods like anisotropic regularization[13] and total-variation-based[14] regularization methods, as well as maximum-likelihood image deblur algorithms,[15] are also able to restore the blurred images.

One method to improve the estimation results is by using two or more blurred images of the same scene.[10,16] Yuan et al.[17] incorporate additional unblurred noisy images to improve the estimation results. Recently, the methods based on a single blurred image have tended to deploy more effective priors for deblurring. Heavy-tailed distributions,[18,19] sparse approximation,[20] transparency,[21] and sharp edge characteristics,[22] are reported to be good priors for natural-scene image blind deconvolution.

The proposed method for blind deconvolution also uses heavy-tailed distribution priors, but it differs from previous methods in two respects. First, we employ a histogram remapping method to correct the gradient distribution function. Secondly, the kernel elements are represented by a sigmoid function, and the kernel is estimated in the gradient domain. In order to solve the involved optimization problem efficiently, we have developed new methods to estimate the kernel and the latent image. They constitute another contribution of this paper.

The paper is organized as follows. In Sec. 2, the related works are reviewed. The histogram remapping method adopted in this paper is also discussed. In Sec. 3, we present the proposed model for image deblurring and kernel estimation. The subproblems involved in the model are detailed in Sec. 3.1. The optimization methods to solve the subproblems are presented in Sec. 4. In Sec. 5 the experimental results on synthetic and real blurred images are shown. The conclusions are given in Sec. 6.

2 Related Work

The priors modeling the preference for an unblurred image and the optimization algorithms are the essentials of the blind deconvolution algorithm. Usually, natural scene images are characterized by heavy-tailed distributions.[18] In tight-frame systems, the sparsity of the transformed unblurred image is also prominent.[10] Cai et al.[10,20] demonstrated the efficacy of the deblurring method based on this prior. They solve the corresponding optimization problem by a linearized Bregman iteration method. The Gaussian prior[8] modeling the smoothness of the unblurred image is also researched in previous works. It might be a good method, since it has a closed-form solution. However, the estimated unblurred image tends to be oversmoothed.[23] The hyper-Laplacian prior is more useful for modeling the sparsity,[6,8] but its objective function is more difficult to minimize.

Another method to represent the sparsity is to model the gradient distribution function by a parametric equation.

0091-3286/2010/$25.00 © 2010 SPIE

Fergus et al.[18] use mixtures of Gaussian functions to fit the logarithmic gradient distribution. Shan et al.[19] use the two piecewise concatenated continuous functions to fit the distribution. Modeling the distribution by a parametric equation has the advantage that the parametric equation can be explicitly put into the objective function for blind deconvolution.[19] In both methods, the empirical distributions are all calculated from sharp natural-scene images.

This paper also adopts the heavy-tailed distribution as a prior for the proposed deblur algorithm. However, the empirical distribution is directly deployed during estimation, and its parametric form is not required. The blind deconvolution problem is formulated as a constraint objective function so that the gradients of the latent image are required to match the empirical distribution. During the optimization process, histogram remapping (histogram assignment)[1] is adopted to efficiently correct the distribution function.

2.1 *Histogram Remapping*

Histogram remapping is commonly used for image enhancement. It adjusts the distribution function of image intensity by searching a lookup table.[1] If the cumulative distribution function (CDF) of the target histogram is given, the remapping can be carried out efficiently. In this paper, histogram remapping is performed in the gradient domain. The empirical CDF of the horizontal gradient magnitude is calculated by 50 randomly collected sharp natural-scene images. The function is shown in Fig. 1. The corresponding logarithmic gradient distribution is shown in Fig. 2; it is seen to be a heavy-tailed distribution. During the optimization, the empirical CDF is used to correct the gradient distribution function of the estimated unblurred image by histogram remapping.

3 Our Model

Let the sharp image and blur kernel be f and t, and the blurred image be g. The ideal spatially invariant blur can be represented by convolution, $g = f * t$, where $*$ denotes the image convolution operation. Since the heavy-tailed distribution prior we adopted is based on image gradients, we propose the following constrained objective function for estimating kernel and latent image:

$$J(f,t) = \|f * d_x * t - g_x\|^2 + \|f * d_y * t - g_y\|^2, \qquad (1)$$

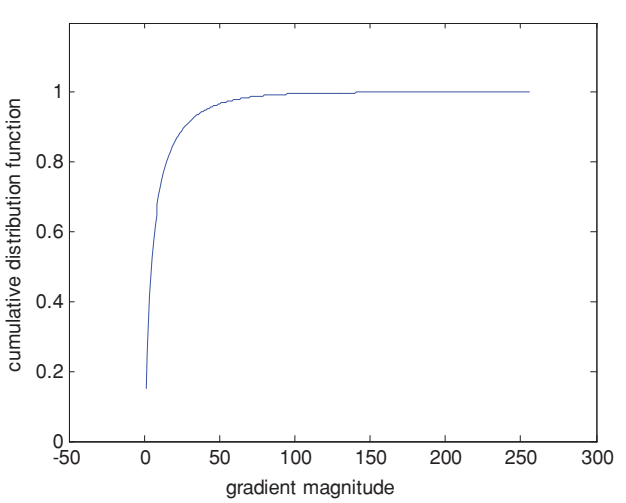

Fig. 1 Cumulative distribution function of the gradient's magnitude.

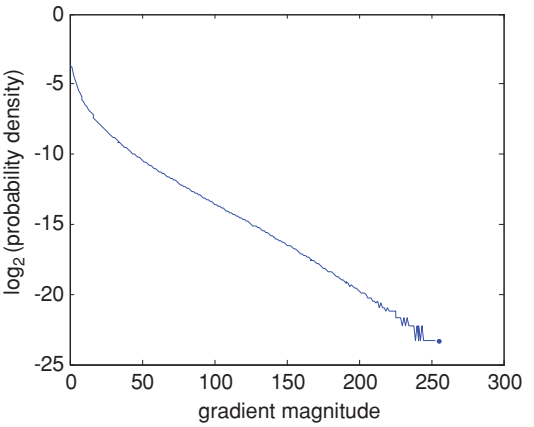

Fig. 2 Logarithmic gradient distribution function calculated from 50 sharp natural images.

subject to the following requirements: (1) Both the horizontal gradients $f_x \triangleq f * d_x$ and the vertical gradients $f_y \triangleq f * d_y$ of the latent image f conform to the empirical distribution. (2) All elements in the kernel t are nonnegative, and their sum equals one.

In Eq. (1), $d_x = [-1, 1]$ and $d_y = [-1, 1]^T$. The images g_x and g_y are the horizontal and vertical gradients of the blurred image. They are computed as $g * d_x$ and $g * d_y$. Although the objective function has a simple form, no closed-form solution exists, due to the constraint conditions. One approach to minimizing (1) might be putting the constraints into the objective function as a penalty function term with an appropriate weight. Then it changes to an unconstrained problem. This procedure coincides with the formulation derived by the Bayesian approach. It tries to maximize the probability $p(\Delta f, t|\Delta g) \propto p(\Delta g|\Delta f, t)p(\Delta f)p(t)$, where the Δ is a gradient operator.

Here $p(t)$ might be customized according to its blurring type. For motion-blurred images, the sparsity of the kernel is a popular prior.[10,16,20,24] But for out-of-focus images, the PSF is commonly modeled by a concrete disk or a Gaussian function. In the proposed objective function, the kernel regularization term is dropped for considering different kinds of blur, and only the physical constraints are considered, namely the non-negativity and the energy preserving property. Experiments showed that our approach is able to suppress the noise in the estimated kernel by the proposed optimization method. Both Gaussian-blurred and motion-blurred images were tested, as presented in Sec. 5.

In order to minimize Eq. (1), we adopt an alternating minimization scheme[6,19] in which f and t are updated alternately. To enforce the constraints on the gradient distribution, f_x and f_y are calculated from the latest estimated f and then corrected by histogram remapping. The corrected gradient images are denoted by f_x^h and f_y^h. They are used to update t and f in the next iteration. This correcting method for solving the constraint optimization problem is similar to the kernel estimation method presented in Refs. 17 and 25, where the constraints on the blur kernel are enforced during optimization. Extensive experiments showed that the, proposed optimization method converges quickly.

Briefly, the proposed method for optimization is carried out iteratively. The values of t, f, f_x^h, and f_y^h are updated in

each iteration. The subproblems for estimating the variables are presented below. The details of solving the subproblems are discussed in Sec. 4.

3.1 *Subproblems of Minimizing the Constraint Objective Function*

3.1.1 *Update t*

Assuming f_x^h and f_y^h have been calculated, we put them into Eq. (1) and get the following function:

$$J(t) = \| f_x^h * t - g_x \|^2 + \| f_y^h * t - g_y \|^2, \quad \text{subject to} \quad 0 \le t_i \le 1, \quad i \in \Omega, \quad \text{and} \quad \sum_{i\in\Omega} t_i = 1. \tag{2}$$

Here Ω is the support of the PSF. This subproblem is also a constraint optimization problem. We developed an corrected gradient descent method to update t. The optimization details are presented in Sec. 4.1.

3.1.2 *Update f*

Holding t constant, Eq. (1) could be minimized easily by traditional nonblind deconvolution methods. However, the kernel t is noisy during iterations. The estimated f might be filled with rings. To suppress the rings and let the gradient image of f approach the empirical distribution, f_x^h and f_y^h are incorporated to update f. The objective function for updating f is formulated as

$$J(f) = \| f * t_x - g_x \|^2 + \| f * t_y - g_y \|^2 + \lambda \| f * d_x - f_x^h \|^2 + \lambda \| f * d_y - f_y^h \|^2, \tag{3}$$

where $t_x = d_x * t, t_y = d_y * t$. We use the default value $\lambda = 0.01$ in our experiments. Note that f_x^h and f_y^h are constants, which also have been used to update t. An efficient method to solve Eq. (3) is proposed and presented in Sec. 4.2.

3.1.3 *Update f_x^h and f_y^h*

Given the updated f, the horizontal gradient image f_x and vertical gradient image f_y are computed. Next the histogram-remapped versions f_x^h and f_y^h are calculated. The histogram remapping method and the target CDF function have been discussed in Sec. 2.1.

4 Optimization Details

4.1 *Update t*

There are two constraints in Eq. (2). Unlike the interior point method[19] or the Landweber method,[17] we adopt a sigmoid function to represent kernel elements t_i,

$$t_i(\tau_i) = \frac{1}{1 + \exp(-\tau_i)}. \tag{4}$$

Obviously, the kernel element t_i is always nonnegative. Then, t in the function (2) can be replaced by the sigmoid function with parameter τ.

We estimate the kernel in the spatial domain. The convolution operation[1] is considered:

$$g(x, y) = \sum_{p=-a}^{a} \sum_{q=-b}^{b} t(p, q) f(x + p, y + q), \tag{5}$$

where a, b are the height and width of the kernel. It can be simplified as a dot product,[1]

$$g(x, y) = t_v^T f_v(x, y), \tag{6}$$

where $t_v = [t_1, t_2, \ldots, t_K]^T$, $K = (2a + 1)(2b + 1)$. The column vector t_v is reshaped from the kernel matrix t in Eq. (5). The vector $f_v(x, y)$ is stacked from the pixels in the neighborhood of (x, y) in f. According to Eqs. (4) and (6), the function (2) can be rewritten as

$$J(\tau) = \frac{1}{N} \sum_i \left\{ \left[t_v^T f_{x,v}^h(i) - g_x(i) \right]^2 + \left[t_v^T f_{y,v}^h(i) - g_y(i) \right]^2 \right\}, \tag{7}$$

where i is the index of the image coordinate, and N is the number of pixels. The elements of t_v are expressed by the sigmoid function with parameter τ_i. The functions $f_{x,v}^h(i)$ and $f_{y,v}^h(i)$ are column vectors with elements in the neighborhood of i in the images f_x^h and f_y^h. The gradient of Eq. (7) with respect to τ is

$$\frac{\mathrm{d}J(\tau)}{\mathrm{d}\tau} = \frac{\mathrm{d}J(\tau)}{\mathrm{d}t} \cdot \frac{\mathrm{d}t}{\mathrm{d}\tau}, \tag{8}$$

where

$$\frac{\mathrm{d}J(\tau)}{\mathrm{d}t} = \frac{2}{N} \sum_i \left[t_v^T f_{x,v}^h(i) - g_x(i) \right] f_{x,v}^h(i) + \frac{2}{N} \sum_i \left[t_v^T f_{y,v}^h(i) - g_y(i) \right] f_{y,v}^h(i),$$

and for each kernel element, $\mathrm{d}t_i/\mathrm{d}\tau_i = t_i^2 \exp(-\tau_i)$.

To minimize Eq. (7), τ_i is updated by the standard gradient descent method and t_i is updated later. To meet the second constraint on t_i, we normalize it by

$$t_{i,\text{normalized}} = t_i / s, \quad \text{where} \quad s = \sum_{i=1}^{K} t_i. \tag{9}$$

Basically, there are three steps required to update t in each iteration:

1. Update τ by $\tau \Leftarrow \tau - \mathrm{d}J(\tau)/\mathrm{d}\tau$.
2. Update t by the sigmoid function (4) with the latest τ.
3. Normalize t according to Eq. (9).

4.2 *Update f*

The objective function defined in Eq. (3) could be minimized by the gradient descent method, or by traditional nonblind deconvolution methods. However, we may solve this problem in the frequency domain as described in Refs. 6 and 19. The closed-form solution to this problem is

$$f = \mathsf{F}^{-1}\left(\frac{G_x \circ T_x^* + G_y \circ T_y^* + \lambda F_x^h \circ D_x^* + \lambda F_y^h \circ D_y^*}{T_x \circ T_x^* + T_y \circ T_y^* + \lambda D_x \circ D_x^* + \lambda D_y \circ D_y^*} \right), \tag{10}$$

where * means the complex conjugate, $\circ$ denotes component-wise multiplication, F^{-1} denotes inverse Fourier transformation, and G_x, G_y, T_x, T_y, F_x^h, F_y^h, D_x, and D_y are the Fourier transforms of g_x, g_y, t_x, t_y, f_x^h, f_y^h, d_x, and d_y, respectively. In each iteration, only the Fourier transforms of f_x^h, f_y^h, and

t need to be computed. The rest all can be precomputed (T_x is multiplied by T and D_x; T_y is multiplied by T and D_y).

Experiments show that the terms $\lambda\|f * d_x - f_x^h\|^2 + \lambda\|f * d_y - f_y^h\|^2$ in Eq. (3) are effective in suppressing rings. Some components of $T_x \circ T_x^* + T_y \circ T_y^*$ in Eq. (10) may be very small. Then the resulting divided spectrum could be degraded by high-frequency noise without the terms $\lambda D_x \circ D_x^* + \lambda D_y \circ D_y^*$.

4.3 *Summary of the Whole Algorithm*

The proposed method for blind deblurring is summarized as follows:

Algorithm 1. Image deblur in gradient domain.

Require: The blurred image g.

Initialization:

Compute gradient image g_x, g_y.

Let $f_x = g_x$, $f_y = g_y$.

Kernel t is initialized as a 2-D Gaussian function.

Repeat

a. Histogram-remap f_x, f_y; the results are denoted by f_x^h, f_y^h.

b. Update kernel by gradient descent method. Three steps are involved:
   - Update τ by $\tau \Leftarrow \tau - \mathrm{d}J(\tau)/\mathrm{d}\tau$.
   - Update t by the sigmoid function (4) with estimated τ.
   - Normalize t according to Eq. (9).

c. Compute f by Eq. (10).

d. Compute the gradient images f_x and f_y based on the updated f.

Until they have converged or the maximum number of iterations of have been performed.

Return f and t.

In our experiments, the convergence is measured by the $L1$ norm of the difference between the consecutive estimates of t with threshold $1e-5$. The maximum number of iterations is 50. The standard deviation of the 2-D Gaussian function to initialize the kernel is a quarter of the kernel width. To avoid local minima, the multiscale approach described in Ref. 18 is adopted. The kernel is estimated in a coarse-to-fine manner, and its initial size is specified by the user.

5 Experiments

The proposed algorithm was implemented in C++ and tested on a Windows PC with an Intel 2.6-GHz CPU. To evaluate the performance of the algorithm, both synthetic and real blurred images were tested. The experimental results produced by Fergus et al.'s[18] code were compared in the experiments. We used the authors' code and hand-tuned the parameters to produce the best possible results.

5.1 *Synthetic Images*

In this subsection, we use synthetic blurred images to test the performance of the proposed method. The first example is shown in Fig. 3, where the blurred image (a) is synthesized with a sharp image and a kernel shown in (e). Since the multiscale approach is adopted, three layers are computed in this case (the scale factor is $\sqrt{2}$). The 1st, 5th, and 20th iteration results of the first layer are shown in (b). The next two layers' final estimation results are shown in (c) and (d). The input image is 230×186; the user-specified kernel size is 19×19. Our code takes only 17.5 s. For the same blurred image and kernel size, Shan et al.'s code[19] takes 54 s to

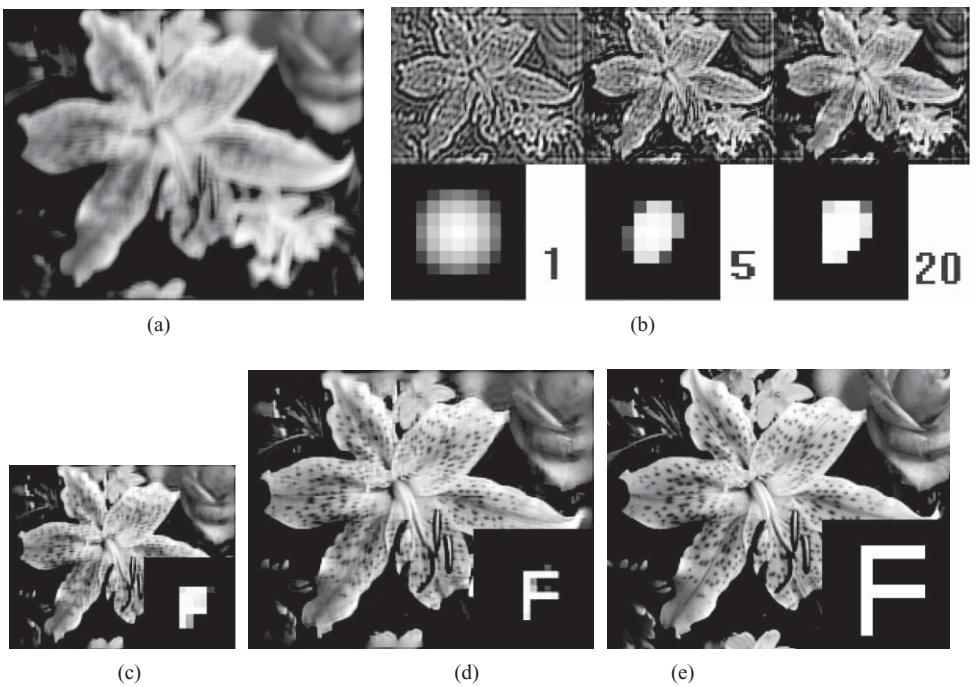

Fig. 3 (a) The input blurred image. (b) The 1st, 5th, and 20th iteration results of the first layer. (c) The 50th estimation result of the second layer. (d) The 50th estimation result of the third layer (the final output). (e) The latent image and the ground truth kernel. (The specified kernel size is larger than the real size.)

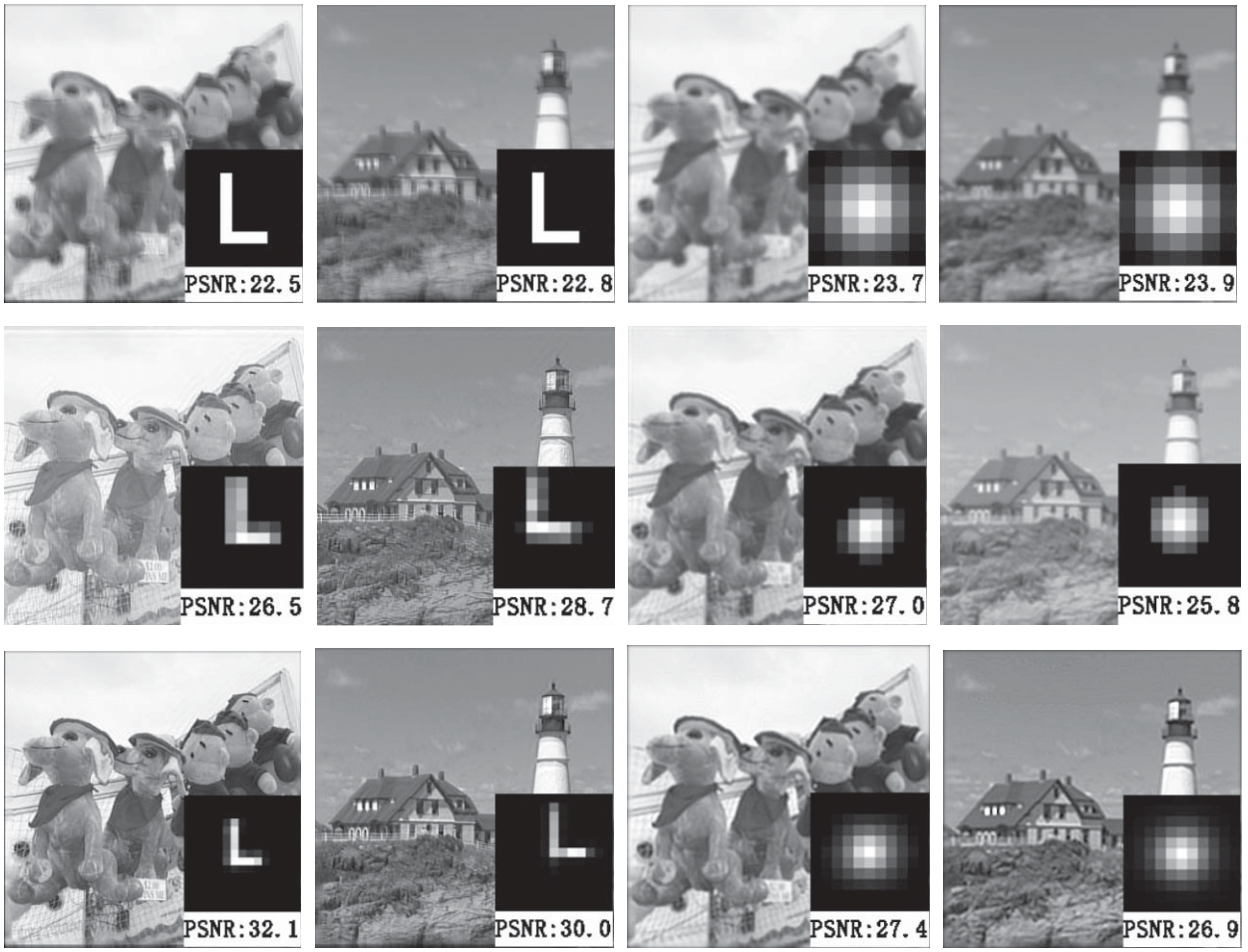

Fig. 4 Motion blur and Gaussian blur examples. The images in the first row are synthesized by convolution. The real kernels and blurred images are presented. The sharp images and kernels estimated by Fergus et al.[18] are presented in the second row. The results estimated by our method are shown in the third row.

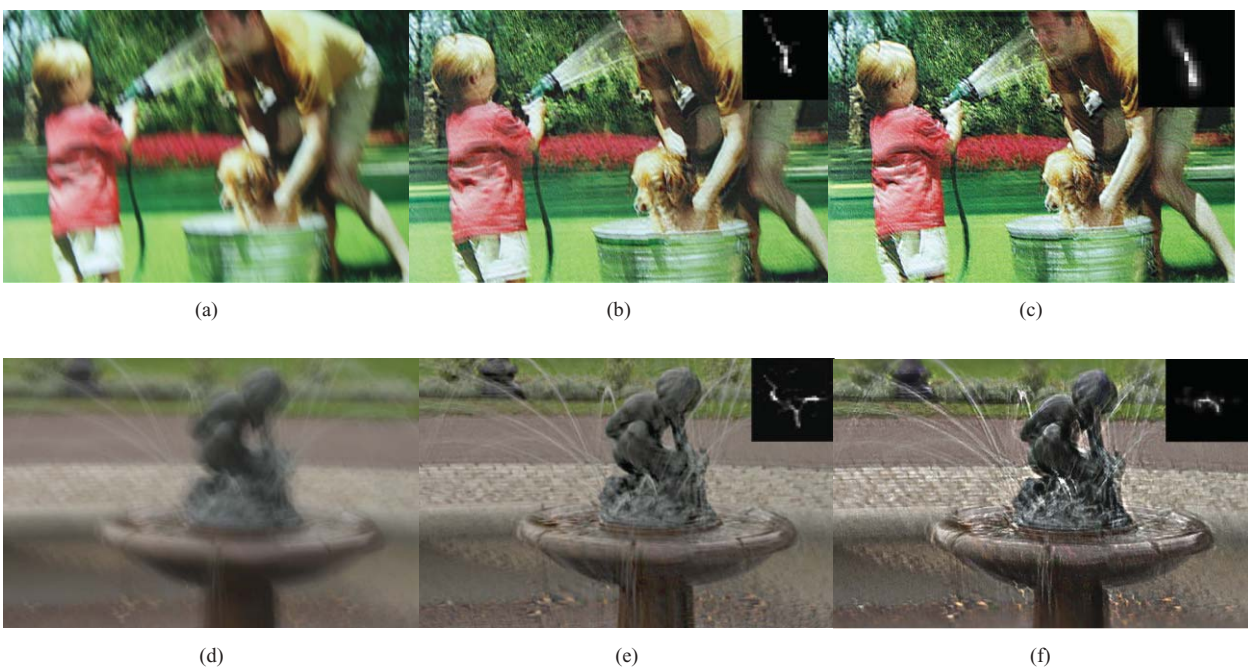

Fig. 5 Experiments on real motion-blurred images. (a), (d) are the blurred images to be restored. (b), (e) are produced by Fergus et al.'s code.[18] (c), (f) are produced by our method.

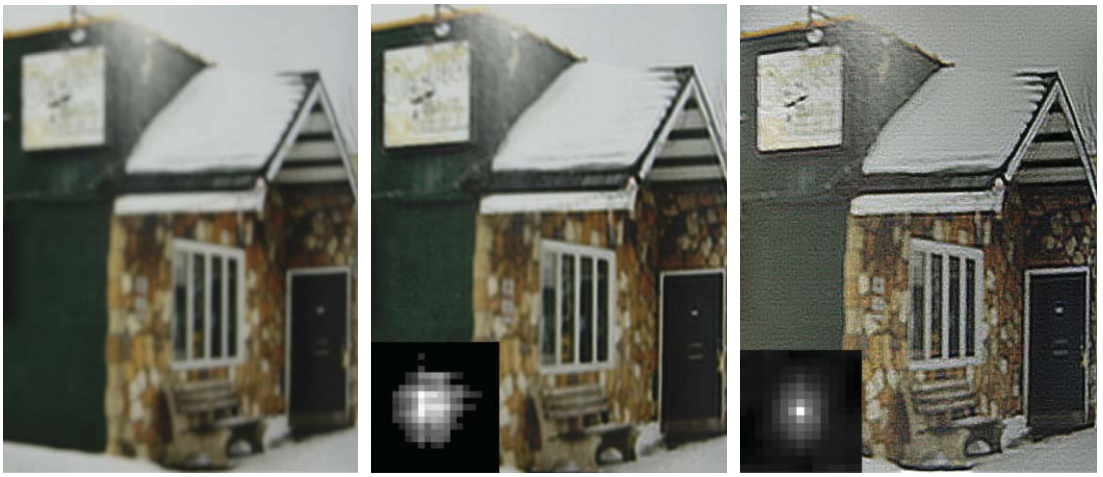

(a) (b) (c)

Fig. 6 Experiments on out-of-focus blur. (a) is an real out-of-focus blurred image. (b), (c) are produced by Fergus et al.'s[18] and our method, respectively.

produce a comparable result, and Fergus et al.'s. MATLAB code[18] takes 8 min.

Figure 4 shows the experimental results on the four synthesized images. Both the motion-blurred and the Gaussian-blurred images are tested. The synthetic blurred images and real PSFs are shown in the first row of the figure. The images and PSFs in the second row are those estimated by Fergus et al.[18] The results produced by our method are shown in the third row. The peak SNRs of (PSNRs) of the images are calculated from the image shown and the corresponding unblurred image. It is observed that all the PSFs have been well reconstructed. However, the PSNRs of the images on the last two columns restored by the proposed method are not as high as the PSNRs of the left two images. That is because of the lowpass filter effect of the Gaussian function. Actually, the killed high-frequency energies of Gaussian blurred images are difficult to restore by a deconvolution method even if the ground truth PSF is used for nonblind deconvolution.

5.2 *Real Blurred Images*

It is challenging to deblur real images, for several reasons. Firstly, a spatially invariant model is the basic assumption for common blind deblur algorithms,[10,18,19] and it is apt to be violated in real circumstances, as stated in Ref. 23. Secondly, the noise embedded in the blurred images makes the estimation problem difficult. In this subsection, we show some examples where real blurred images are restored by the proposed algorithm. The results produced by Fergus et al.'s code[18] are also compared.

In the experiments, color images are converted to grayscale images for kernel estimation. Then the three channels of the color images are simply restored by Wiener filtering.[1] In Fig. 5, experiments on two motion-blurred images are shown. Both images are blurred by complex motion. Figure 6 shows an experiment on out-of-focus blur. It is observed that the deblurred images produced by our method are sharp. It should be noted that the proposed method is just based on the gradients of the input blurred image, and the deblurred color images are computed by Wiener filtering. Other nonblind deconvolution methods[6,7] would further improve the results.

6 Discussion

This paper proposes a new method for blind deconvolution of images. Kernel estimation is carried out in the gradient domain, and a histogram remapping method is adopted to correct the gradient distribution of the estimated image. To the best of our knowledge, no histogram remapping method has been deployed for image deblurring previously. Experiments showed that the proposed method is faster than traditional methods and it is able to restore both out-of-focus images and complex motion-blurred images.

A minor additional difference between the proposed method and the previous methods is that the kernel prior is dropped in our method. Actually, we also tried the exponential distribution prior[19] for kernel estimation, which is implemented by a gradient descent method. However, the prior makes little contribution to the experimental results. One reason is that the kernel elements are represented by a sigmoid function, which is another novelty of the proposed method. It always keeps kernel elements nonnegative and gives a good constraint to the kernel estimation algorithm.

Acknowledgments

The authors would like to thank the anonymous reviewers and editors, whose comments and suggestions greatly improved the manuscript, and also thank Yin Li for his constructive comments. The research is supported by the Foundation 2009DFA12870 international cooperative project (China–New Zealand), supported in turn by the Ministry of Science and Technology, China; and by the Foundation 09410700700 international cooperative project (Shanghai–Rohne Alpens), supported in turn by the Committee of Science and Technology, Shanghai.

References

1. R. C. Gonzalez and R. E. Woods,*Digital Image Processing*, Pearson Education (2003).
2. L. B. Lucy, "An iterative technique for the rectification of observed distributions," *Astron. J.* **79**, 745–754 (1974).
3. W. H. Richardson, "Bayesian-based iterative method of image restoration," *J. Opt. Soc. Am. A* **62**, 55–59 (1972).
4. R. J. Hanisch, R. L. White, and R. L. Gilliland, *Deconvolution of Images and Spectra*, Academic Press (1997).

5. S. Schuon and K. Diepold, "Comparison of motion de-blur algorithms and real world deployment," *Acta Astronautica* **64**, 1050–1065 (2009).
6. D. Krishnan and R. Fergus, "Fast image deconvolution using hyper-Laplacian priors," in *Advances in Neural Information Processing Systems* (2009).
7. N. Joshi, C. Zitnick, R. Szeliski, and D. Kriegman, "Image deblurring and denoising using color priors," in *Proc. IEEE Conf. on Computer Vision and Pattern Recognition* (2009).
8. A. Levin, R. Fergus, F. Durand, and W. T. Freeman, "Image and depth from a conventional camera with a coded aperture," *ACM Trans. Graph.* **26**(3), 70:1–70:9 (2007).
9. L. Yuan, J. Sun, L. Quan, and H. Shum, "Progressive inter-scale and intra-scale non-blind image deconvolution," in *Proc. ACM SIGGRAPH 2008, ACM Trans. Graph.* **27**, No. 3 (2008).
10. J. Cai, H. Ji, C. Liu, and Z. Shen, "High-quality curvelet-based motion deblurring from an image pair," in *Proc. IEEE Conf. on Computer Vision and Pattern Recognition* (2009).
11. J. Biemond, R. Lagendijk, and R. Mersereau, "Iterative methods for image deblurring," *Proc. IEEE* **78**(5), 856–883 (1990).
12. Y. Yitzhaky and N. S. Kopeika, "Identification of blur parameters from motion blurred images," *Graph. Models Image Process.* **59**(5), 310–320 (1997).
13. Y. You and M. Kaveh, "Blind image restoration by anisotropic regularization," *IEEE Trans. Image Process.* **8**(3), 396–407 (1999).
14. T. F. Chan and C. K. Wong, "Total variation blind deconvolution," *IEEE Trans. Image Process.* **7**(3), 370–375 (1998).
15. R. L. Lagendijk, A. M. Tekalp, and J. Biemond, "Maximum likelihood image and blur identification: a unifying approach," *Opt. Eng.* **29**, 422–435 (1990).
16. J. Chen, L. Yuan, C. Tang, and L. Quan, "Robust dual motion deblurring," in *Proc. IEEE Conf. on Computer Vision and Pattern Recognition* (2008).
17. L. Yuan, J. Sun, L. Quan, and H. Shum, "Image deblurring with blurred/noisy image pairs," in *Proc. ACM SIGGRAPH 2007, ACM Trans. Graph.* **26**, No. 3 (2007).
18. R. Fergus, B. Singh, A. Hertzmann, S. T. Roweis, and W. T. Freeman, "Removing camera shake from a single photograph," *ACM Trans. Graph.* **25**(3), 787–794 (2006).
19. Q. Shan, J. Jia, and A. Agarwala, "High-quality motion deblurring from a single image," in *Proc. ACM SIGGRAPH 2008, ACM Trans. Graph.* **27**, No. 3 (2008).
20. J. Cai, H. Ji, C. Liu, and Z. Shen, "Blind motion deblurring from a single image using sparse approximation," in *Proc. IEEE Conf. on Computer Vision and Pattern Recognition* (2009).
21. J. Jia, "Single image motion deblurring using transparency," in *Proc. IEEE Conf. on Computer Vision and Pattern Recognition* (2007).
22. N. Joshi, R. Szeliski, and D. Kriegman, "PSF estimation using sharp edge prediction," in *Proc. IEEE Conf. on Computer Vision and Pattern Recognition* (2008).
23. A. Levin, Y. Weiss, F. Durand, and W. T. Freeman, "Understanding and evaluating blind deconvolution algorithms," in *Proc. IEEE Conf. on Computer Vision and Pattern Recognition* (2009).
24. L. Yuan, J. Sun, L. Quan, and H. Shum, "Blurred/non-blurred image alignment using an image sequence," in *Proc. ACM SIGGRAPH 2007, ACM Trans. Graph.* **26**, No. 3 (2007).
25. H. W. Engl, M. Hanke, and A. Neubauer, *Regularization of Inverse Problems,* Kluwer Academic (2000).

Xiaogang Chen is a PhD candidate in the Institute of Image Processing and Pattern Recognition, Shanghai Jiao Tong University. His research interests include image restoration, image and video enhancement, and computer vision.

Jie Yang received his PhD in computer science from the University of Hamburg, Germany. He is now a professor and director of the Institute of Image Processing and Pattern Recognition, Shanghai Jiao Tong University. He has led more than 30 national and ministry scientific research projects in image processing, pattern recognition, data amalgamation, data mining, and artificial intelligence, and has published more than 300 research papers.

Qiang Wu received his BEng and MEng degrees in electronic engineering from Harbin Institute of Technology, China, in 1996 and 1998, and his PhD degree in computing science from the University of Technology, Sydney, Australia, in 2004. He joined the School of Computing and Communications, University of Technology, Sydney (UTS), Australia, in 2003, where he is currently a senior lecturer. He has been a member of the iNEXT research center at UTS since 2007. He has published widely on image processing, computer vision, and pattern recognition. His current research interests include object detection, human behavior analysis, biometrics, visual information analysis and retrieval, and spiral architecture. He serves as referee for many conferences and journals. He is a guest editor of *Pattern Recognition Letters* and the *International Journal of Pattern Recognition and Artificial Intelligence*. He is a member of the IEEE.